Effect of Strain Rate and Temperature on the Tensile Properties of MANET II Steel

M.M. Ghoneim

MANET II, a modified 12% Cr steel with the German designation DIN 1.4914, is a candidate structural material for the first wall and blanket in fusion reactors. In the present study, the tensile properties of this steel were investigated in the temperature range of 25 to 350 °C at strain rates of 5×10^{-5}, 1.2×10^{-4}, and $1.2 \times 10^{-3} s^{-1}$. Both microstructure and fracture surfaces were examined using optical and scanning electron microscopic (SEM) techniques. The results showed that the steel suffers dynamic strain aging, although no serrated flow was observed. Yield strength, ultimate strength, and elongation showed negative strain rate sensitivity. Dynamic strain aging also affected the strain hardening rate. Results are discussed with regard to the chemical composition and fracture surface morphology.

Keywords Cr steels, dynamic strain aging, fusion reactor materials, MANET steel

1. Introduction

Ferritic/martensitic 9-12% Cr 1% Mo steels are extensively used as structural materials for service at elevated temperatures in the petroleum and chemical industries and in conventional power stations (Ref 1). In the nuclear industry, modifications of these steels are attractive candidates for structural materials in fast breeder reactors and fusion reactors. The interest in these alloys is due to high resistance to irradiation-induced swelling and creep and low thermal expansion properties compared to austenitic stainless steels (Ref 1, 2).

Within the European community, a martensitic DIN 1.4914 CrNiMoVNb steel was chosen as a possible first wall and blanket material for the fusion reactors and was designated martensitic alloy for next European torus (MANET) (Ref 3).

Extensive research work has been completed to study the phenomenon of dynamic strain aging in steels because of its effects on mechanical properties, mainly the increase in flow stress, decrease in ductility, and fracture toughness (Ref 4). Dynamic strain aging was reported in a wide range of steels, including mild steel, ferritic and austenitic stainless steels, maraging steels, and chromium steels (Ref 4-6). The 9-12% Cr steels were found to exhibit dynamic strain aging (Ref 7-10). However, published data referring to this are limited.

While the tensile properties of the 1.4914 MANET II steel were investigated (Ref 3), the effect of the strain rate on these properties was not studied. In the present study, the influence of strain rate and temperature on the tensile properties of MANET II steel was studied.

2. Experimental

The material used in the present investigation, MANET II, was produced by Saarstahl Völklingen, Germany, and was received in the form of a hot-rolled plate of 12 mm thickness. Table 1 gives the chemical composition. The plate was then heat treated using the following method: austenitizing at 1075 °C for 0.5 h, air cooling, followed by temperature at 750 °C for 2 h, and air cooling.

Tensile specimens with gage lengths of 60 mm and diameters of 6 mm (DIN 50125) were manufactured in the transverse (TL) direction. Tests were carried out in air in the temperature range of 25 to 350 °C at strain rates of 5×10^{-5}, 1.2×10^{-4}, and $1.2 \times 10^{-3} s^{-1}$ using an Instron universal testing machine, model 1185. The machine was operated under displacement control, and the strain rates given in this work are nominal values based on the cross-head velocity and the initial specimen dimensions. Each specimen was held for approximately 15 min at the testing temperature before testing began. The temperature was controlled to within ±2 °C. The load-elongation curves were analyzed to determine the yield strength (0.2% offset), ultimate strength, uniform and total elongation, and work hardening rate.

Microstructural examination was done using optical metallography of polished and etched sections. The etchant was 400 mL ethanol + 50 mL HCl + 50 mL HNO_3 + 6 g picric acid, and the etching time was 20 to 30 s. Scanning electron microscopy (SEM) was used to examine the fracture surface of specimens representing the various testing conditions.

3. Results and Discussion

Figure 1 shows the microstructure of the investigated material. It consists of fully tempered martensite with elongated laths. The prior austenite grain size is approximately 25 μm. The grain boundaries and the interlath boundaries are heavily precipitated with $M_{23}C_6$ carbides (Ref 3).

Figures 2 and 3 show typical examples of the load-elongation curves obtained from the tensile tests. In general, the curves were almost smooth at all testing temperatures and strain rates. Rarely, small irregularities were noticed. No serrations were observed. However, examination of the curves obtained at different temperatures (Fig. 2) or different strain rates (Fig. 3) revealed indications of dynamic strain aging. This is shown in the following sections.

3.1 *Strength and Ductility*

Figure 4 shows the variation of yield strength (open symbols) and ultimate strength (closed symbols) with testing tem-

M.M. Ghoneim, Atomc Energy Authority, Cairo, Egypt.

perature and strain rate. The strength decreases gradually with the increase in temperature from 25 to 250 °C. For the highest strain rate used, $1.2 \times 10^{-3} s^{-1}$, the strength values continued to decrease in the range of 250 to 350 °C. However, for the other strain rates, 5×10^{-5} and $1.2 \times 10^{-4} s^{-1}$, both yield and ultimate strengths were nearly constant in this temperature range. A maximum value was reached at 300 °C. At room temperature, the strength increased with an increase of the strain rate. On the contrary, at 300 and 350 °C, both yield and ultimate strengths increased with decreasing strain rate, indicating negative strain rate sensitivity.

The effect of testing temperature and strain rate on ductility (elongation) is shown in Fig. 5. Elongation decreased with increasing testing temperature at all strain rates. At room temperature, elongation increased slightly with decreasing strain rate. However, at 250, 300, and 350 °C, elongation decreased with decreasing strain rate. Examination of the results in Fig. 5 shows that the decrease in total elongation (closed symbols) was due to the reduction in uniform elongation (open symbols). At the strain rate of $1.2 \times 10^{-4} s^{-1}$, the uniform elongation decreased from 6.5% at 25 °C to 2.5% at 350 °C. The corresponding values of total elongation are 12.2 and 7.1%, respectively. This means that the reduction in uniform elongation represents approximately 80% of the reduction in total elongation. Similar results can be obtained when considering the effect of the strain rate at constant testing temperatures such as 250, 300, and 350 °C. On average, the reduction in uniform elongation represented approximately 85% of the reduction in total elongation.

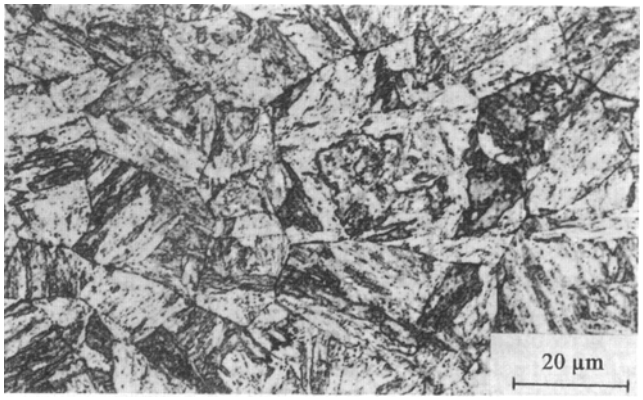

Fig. 1 Microstructure of 1.4914 MANET II steel austenized at 1075 °C/0.5 h, air cooling, tempered at 750 °C for 2 h, and air cooling

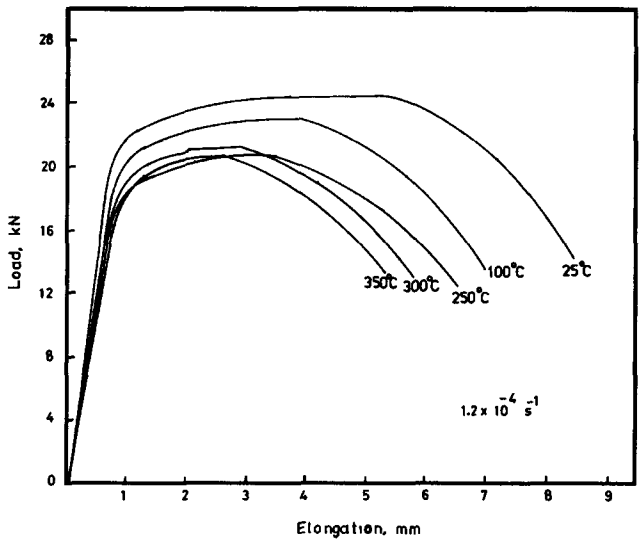

Fig. 2 Effect of test temperature on load-elongation curves at a constant strain rate of $1.2 \times 10^{-4} s^{-1}$

The above results, that is, negative strain rate sensitivity of the flow strength and decrease in ductility, indicate that the investigated material suffers dynamic strain aging, although no serrated flow was noticed. Dynamic strain aging in body-centered cubic (bcc) metals is related to dynamic interaction between interstitial carbon and nitrogen atoms and mobile dislocations. Based on activation energy considerations, diffusing carbon atoms are responsible for dynamic strain aging in 9Cr-1Mo steels (Ref 7, 8). However, because the activation energy for diffusion of carbon and nitrogen in α-iron does not differ markedly, it is difficult to identify from the activation energy measurement the particular interstitial atom responsible for the occurrence of dynamic strain aging (Ref 11).

The dynamic strain aging effect is expected to be weak in the investigated material due to high-alloying element content and the presence of strong carbide and nitride formers (zirconium, niobium, and vanadium). Therefore, most interstitial carbon and nitrogen are expected to be removed from the solution and precipitate as carbides and nitrides (Ref 4). In addition, it was reported (Ref 12) that in contrast to mild steel, dislocations in martensite never become strongly pinned by strain aging. The dislocation atmospheres are more diluted in martensite than in ferrite, and the pinning is correspondingly weaker. Therefore, in the investigated material, the serrations, if present, are expected to be of a very small amplitude. Possibly, the testing system was not suitable to record such weak serrations.

Serrated flow was reported for a preceding version (MANET I) of the investigated steel (Ref 9, 10). In the first study (Ref 9), the strain rate was $1.2 \times 10^{-4} s^{-1}$, and serrated flow was observed between 280 and 350 °C. In the second study (Ref 10), the strain rate was approximately $2.5 \times 10^{-4} s^{-1}$, and serrated flow was observed in the temperature range of 250

Table 1 Chemical composition of 1.4914 MANET II steel

Element	Composition, wt%
C	0.10
Si	0.18
Mn	0.76
P	0.004
S	0.005
Cr	10.37
Ni	0.65
Mo	0.58
V	0.21
Nb	0.16
B	0.0075
N	0.032
Al	0.007
Co	0.005
Cu	0.01
Zr	0.008

to 350 °C. However, there was no information in these studies concerning the amplitude of the serrations.

On the other hand, dynamic strain aging without serrations was observed in several cases (Ref 13, 14). Baird (Ref 12) discussed the case where both serrated and smooth flow are present in the stress-strain curve. Baird (Ref 12) proposed the probability that the only difference between the two types of flow is that serrations mark the occasions where inhomogeneous bursts of deformation spread catastrophically across the entire specimen producing appreciable drops in stress. In the homogeneous ranges, the irregularities are confined to grains and cancel out, giving apparently smooth stress-strain curves.

3.2 *Work Hardening*

The average work hardening rate θ was calculated as:

$$\theta = \frac{\Delta\sigma}{\Delta\varepsilon} \qquad \text{(Eq 1)}$$

where σ and ε are the true stress and true strain, respectively. This average was calculated for two plastic strain stages; the first stage is for ε = 0.002 to 0.01, and the second stage is for ε = 0.01 to 0.02. Figure 6 shows the results. The normal behavior is that the work hardening rate decreases with increasing strain and testing temperature. Figure 6 shows that the work hardening rate decreased with an increase in strain for all testing temperatures. However, the response to the variation in the testing temperature was dependent on the strain level. At the beginning of the plastic deformation, 0.002 to 0.01 strain (open symbols), the strain hardening rate at 250, 300, and 350 °C (the dynamic strain aging range) was higher than that at 25 °C. Conversely, for the strain range 0.01 to 0.02 (closed symbols), the

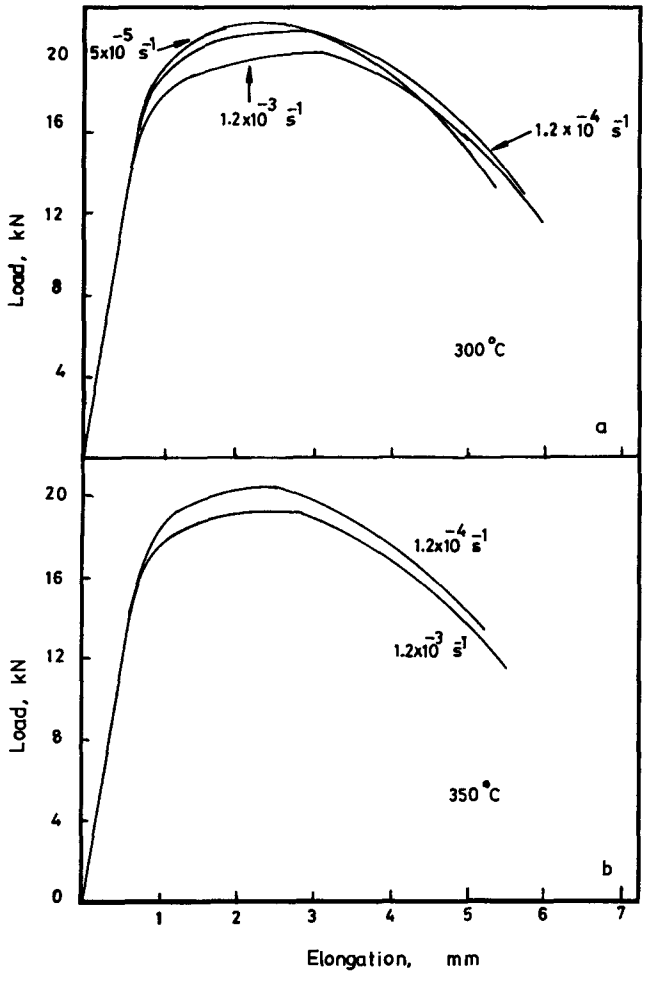

Fig. 3 The effect of strain rate on the load-elongation curves at constant test temperature. (a) 300 °C. (b) 350 °C

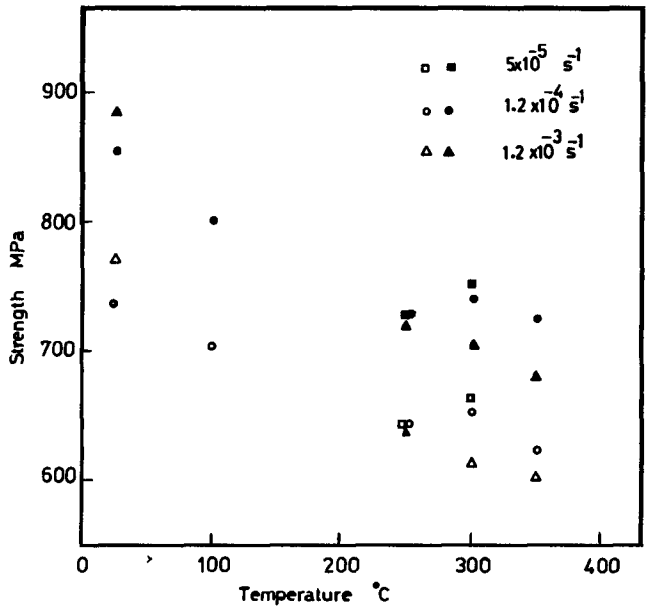

Fig. 4 Effect of strain rate and test temperature on yield strength (open symbols) and ultimate strength (closed symbols)

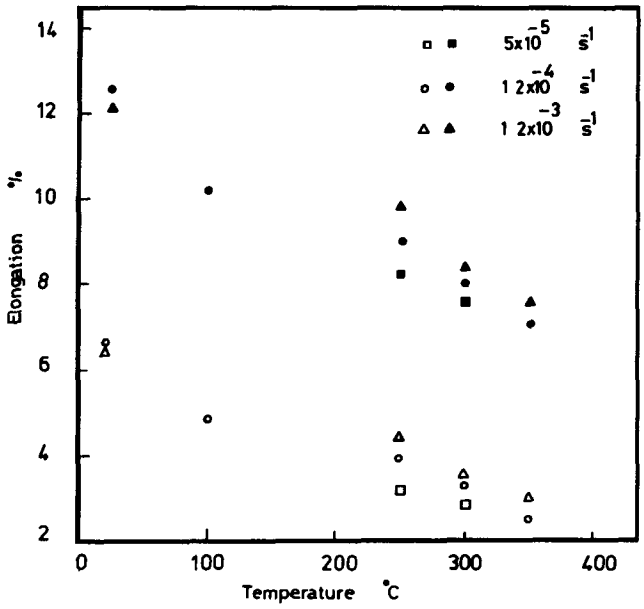

Fig. 5 Effect of strain rate and test temperature on uniform elongation (open symbols) and total elongation (closed symbols)

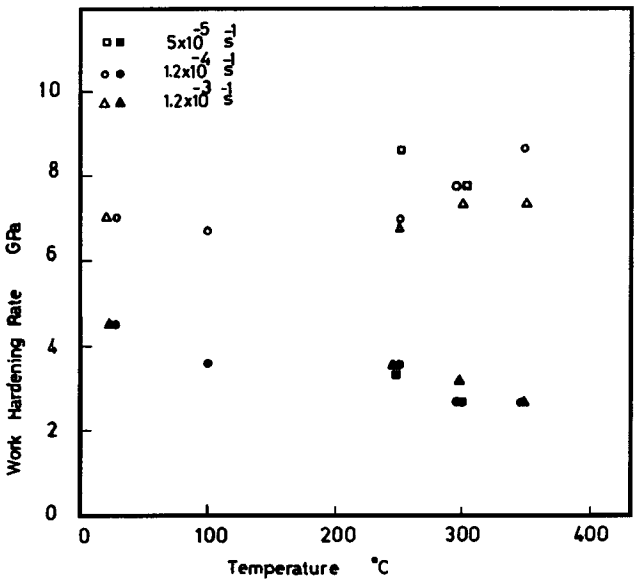

Fig. 6 Effect of strain rate and test temperature on the average work hardening rate. Open symbols represent $\varepsilon = 0.002$ to 0.01, while closed symbols represent $\varepsilon = 0.01$ to 0.02

work hardening rate decreased with increasing testing temperature in the entire range studied.

The above noted behavior of hardening rate in the presence of dynamic strain aging can be explained as follows. During straining, the dynamic strain aging initially increases the strain hardening rate. This is attributed to the increase in dislocation density in the dynamic strain aging temperature range (Ref 4). Due to the pinning of dislocations by solute atoms, fresh dislocations are continually formed to maintain the applied strain rate. In addition, the rate of elimination of dislocations by mutual annihilation decreases. However, as mentioned previously, the available interstitial carbon and nitrogen are low in the studied material. Therefore, with increasing deformation the supply of interstitial atoms, for interaction with dislocations, becomes depleted, and the hardening rate falls. Similar cases were reported previously (Ref 15).

The decrease in the uniform elongation illustrated in Fig. 5 is a consequence of the initial increase and, thereafter, the decrease in hardening rate. In the tensile test (Ref 15), the uniform strain becomes unstable, and necking begins when the strain hardening rate becomes equal to the flow stress, that is, when

$$\frac{\Delta\sigma}{\Delta\varepsilon} = \sigma \qquad \text{(Eq 2)}$$

The increase in yield strength (Fig. 4) and the initial increase in hardening rate due to dynamic strain aging raise the flow strength. However, the hardening rate falls again, thus leading to the equality required by Eq 2. The resultant effect is a drop in the uniform elongation.

3.3 *Fractography*

Figures 7 and 8 show typical examples of scanning electron microscopy (SEM) fractographs. On the microscopic scale, all the specimens showed ductile dimple fracture independent of the testing temperature or the strain rate. On the macroscopic scale, the specimens tested at 100, 250, 300, and 350 °C showed ordinary cup and cone fractures. On the other hand, the specimens tested at 25 °C (Fig. 7a) showed features similar to those termed "milling tool" or "rosette-star" fracture type. In this case, the fracture surface consisted of a fibrous central zone and a radial zone. The radial zone was divided into several zones separated by deep splits. The material within each zone was fractured by shear characterized, in the microscopic scale, with crushed dimples (Fig. 7c) similar to those in the shear lip zone of the cup and cone fractures (Fig. 8c). The central fibrous zone of all the specimens contained typical large and small dimples (Fig. 7b and 8b). However, the dimples in the specimens tested at 25 °C were smaller than those observed at the other temperatures. Because the plain strain constraint is essential in the growth process of the voids, it is believed that the longitudinal separations produced some relaxation of the plain strain constraint.

Since the main difference in the fracture surface features between the specimens tested at 25 °C and those tested at other temperatures is the presence of the radial material separations in the former case, and because the main difference in the tensile properties was the decrease in the uniform elongation in the latter case, it is reasonable to assume that these observations are associated. It is believed that the longitudinal separations initiated at the later stages of the uniform elongation and developed during the early stages of the nonuniform elongation.

The rosette-star fractures were observed before in martensitic microstructures (Ref 16, 17). In the ASM *Metals Handbook* (Ref 16), it was reported that these features are observed only in tensile bars taken parallel to the hot working direction of round-bar stock. On the other hand, these features were observed in specimens, of another heat of the material investigated in the present paper, taken in the longitudinal direction of a rolled plate (Ref 17). However, the specimens in the present study were taken in the transverse direction of a rolled plate.

4. Conclusions

The tensile properties of 1.4914 MANET steel were investigated in the temperature range of 25 to 350 °C at strain rates of 5×10^{-5}, 1.2×10^{-4}, and 1.2×10^{-3} s^{-1}, and the following conclusions were drawn:

- The steel suffers dynamic strain aging in the temperature range of 250 to 350 °C. This is manifested as negative strain rate sensitivity of the yield and ultimate strengths and as a decrease of ductility (elongation). However, the dynamic strain aging effect is weak in this steel, and no serrated flow was observed. This can be attributed to the high-alloying element content.
- The hardening rate in the dynamic strain aging range depends on the plastic strain level. At the beginning of the plastic deformation, dynamic strain aging causes the average hardening rate to increase. However, at higher strain levels, this rate falls again due to depletion of the interstitial atoms.

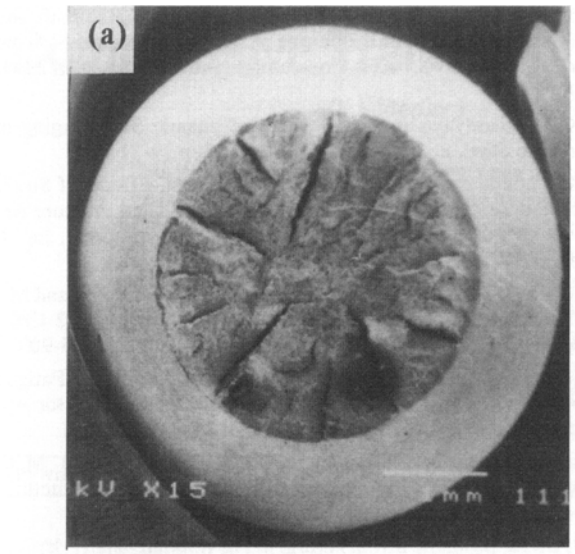

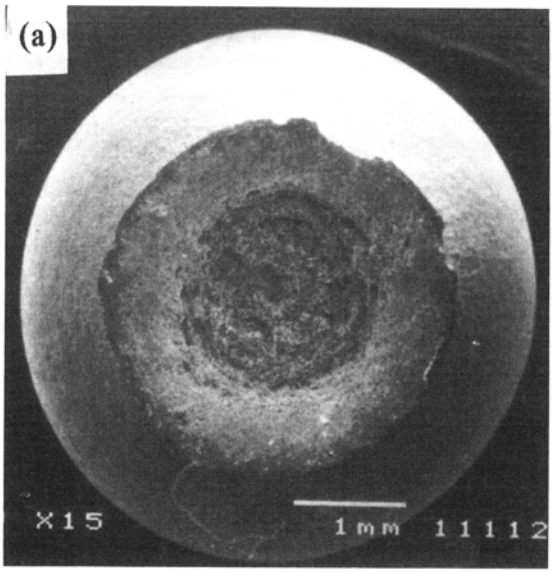

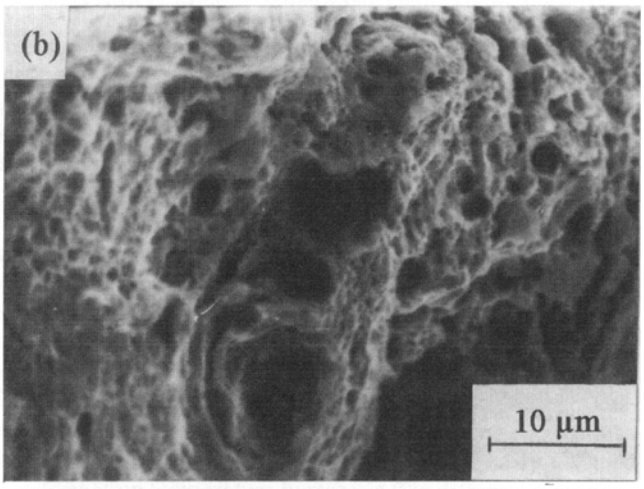

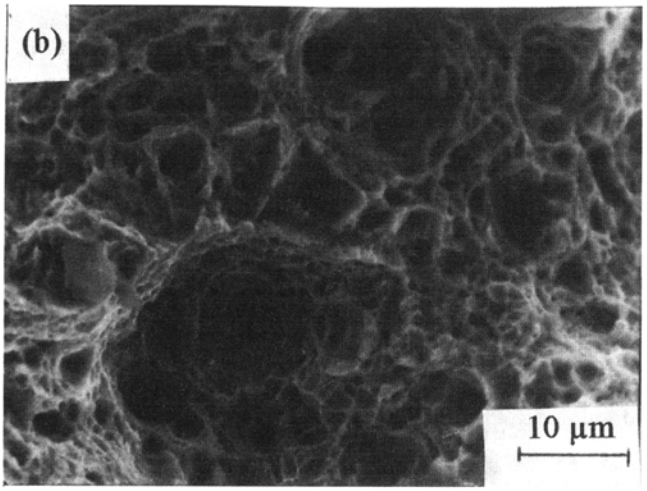

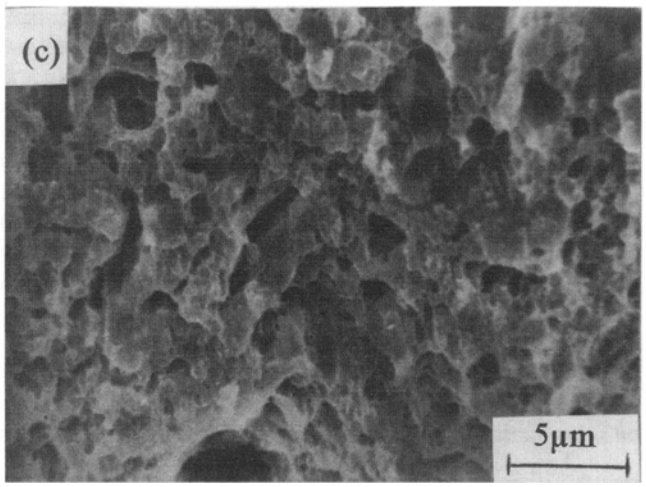

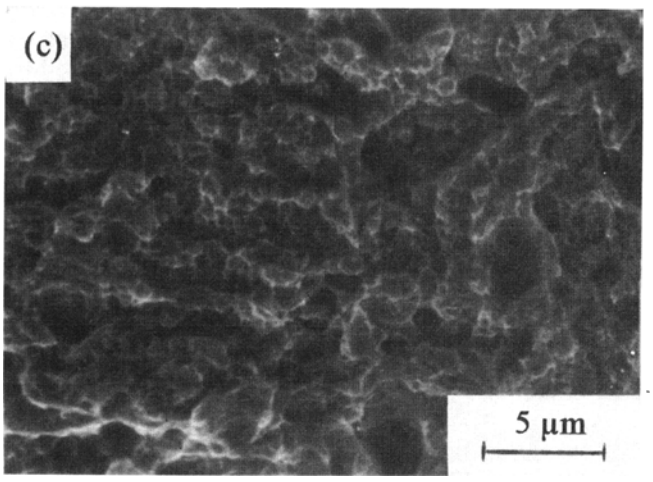

Fig. 7 Typical scanning electron micrograph fractographs of MANET II steel tensile specimens tested at 25 °C. (a) Macroscopic. (b) Central fibrous zone. (c) Radial zone

Fig. 8 Typical scanning electron micrograph fractographs of MANET II steel tensile specimens tested at 300 °C. (a) Macroscopic. (b) Central fibrous zone. (c) Shear lip zone

- The reduction in the total elongation is due to the reduction in the uniform elongation. This reduction in uniform elongation can be ascribed to the effect of dynamic strain aging on the work hardening rate.
- Ductile dimple is the mode of fracture in the testing temperature range of 25 to 350 °C. However, the fracture surface at 25 °C is characterized by the presence of deep radial material separations, similar to those of the milling tool or rosette-star types of fracture, while at 100 to 350 °C, ordinary cup and cone fractures are observed.

Acknowledgments

The author would like to thank the International Atomic Energy Agency (IAEA) and Prof. Dr. D. Munz, the director of IMF II, KfK Research Centre, Karlsruhe, Germany. This work was conducted while the author was on an IAEA fellowship at KfK.

References

1. J. Orr, F.R. Beckitt, and G.D. Fawkes, The Physical Metallurgy of Chromium-Molybdenum Steels for Fast Reactor Boilers, in *Ferritic Steels for Fast Reactor Steam Generators,* Vol 1, S.F. Pugh and E.A. Little, Ed., BNES, London, 1978, p 91-109
2. R.L. Klueh, K. Ehrlich, and F. Abe, Ferritic/Martensitic Steels: Promises and Problem, *J. Nucl. Mater.,* Vol 191-194, 1992, p 116-124
3. M. Schirra, P. Graf, S. Heger, H. Meinzer, W. Schweiger, and H. Zimmermann, "MANET II: Untersuchngsergebnisse zum Umwandlungs-und Vergütungsverhalten und Prüfung Mechanischer Eigenschaften," KfK Report 5177, May 1993
4. J.D. Baird, The Effects of Strain Aging Due to Interstitial Solutes on the Mechanical Properties of Metals, Review 149, *Metall. Rev.,* Vol 5, 1971, p 1-18
5. L.H. de Almeida, P.R.O. Emygdio, and I. Le May, Activation Energy Calculation and Dynamic Strain Aging in Austenitic Stainless Steel, *Scr. Metall. Mater.,* Vol 31 (No. 5), 1994, p 505-510
6. M.E. Abd El-Azim, P.J. Ennis, H.S. Schuster, F.H. Hammad, and H. Nickel, "The Tensile Properties of Alloys 800H and 617 in the Range 20 to 950 °C," KFA Forschungszentrum Report Jül 2344, 1990
7. R.K. Upadadhyaya and M.N. Shetty, Dynamic Strain Aging in 9Cr-1Mo Steel, *Z. Metallkd.,* Vol 82, 1991, p 19-21
8. B.K. Choudhary, K.B. Rao, and S.L. Mannan, Effects of Strain Rate and Temperature on Tensile Deformation and Fracture Behavior of Forged Thick Section 9Cr-1Mo Ferritic Steel, *Int. J. Pressure Vessels Piping,* Vol 58, 1994, p 151-160
9. K.K. Bae, K. Ehrlich, and A. Möslang, Tensile Behavior and Microstructure of the Helium and Hydrogen Implanted 12 Cr%-Steel MANET, *J. Nucl. Mater.,* Vol 191-194, 1992, p 905-909
10. P. Marmy, R. Yuzhen, and M. Victoria, The Tensile and Fatigue Properties of Type 1.4914 Ferritic Steel for Fusion Reactor Applications, *J. Nucl. Mater.,* Vol 179-181, 1991, p 697-701
11. J.K. Chakravartty, S.L. Wadekar, T.K. Sinha, and M.K. Asundi, Dynamic Strain Aging of A203D Nuclear Structural Steel, *J. Nucl. Mater.,* Vol 119, 1983, p 51-58
12. J.D. Baird, Dynamic Strain Aging, in *The Inhomogeneity of Plastic Deformation,* American Society for Metals, 1973, p 191-222
13. S.T. Mahmoud, K.M. Al-Otaibi, Y.H. Yung, and K.L. Murty, Dynamic Strain Aging and Neutron Irradiation Effects on Mechanical and Fracture Properties of A533B Class 1 PV Steel and 2.25Cr-1Mo Steel, *J. Test. Eval.,* Sept 1990, p 332-337
14. K.L. Murty, Interaction of Interstitial Impurities with Radiation-Induced Defects Leading to Improved Elevated Temperature Mechanical Properties of Mild Steel, *Nucl. Technol.,* Vol 67, Oct 1984, p 124-130
15. N.J. Petch and R.W. Armstrong, The Tensile Test, *Acta Metall. Mater.,* Vol 38 (No. 12), 1990, p 2695-2700
16. G.F. Vander Voort, Visual Examination and Light Microscopy, in *Fractography and Atlas of Fractographs,* Vol 9, *Metals Handbook,* 8th ed., American Society for Metals, 1974, p 98-106
17. E. Materna-Morris, M. Schirra, and K. Ehrlich, The Correlation Between Fracture Behavior and Microstructure in Nb-Bearing, Fully Martensitic Steel of Type 1.4914, in *Materials for Nuclear Reactor Core Applications,* BNES, London, 1987, p 263-269